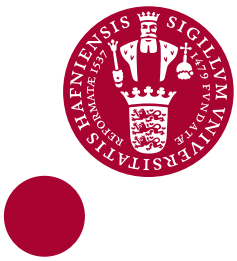

Inducible Degradation of the Human SMC5/6 Complex Reveals an Essential Role Only during Interphase

Venegas, Andrés Bueno; Natsume, Toyoaki; Kanemaki, Masato; Hickson, Ian D.

Published in:
Cell Reports

DOI:
10.1016/j.celrep.2020.107533

Publication date:
2020

Document version
Publisher's PDF, also known as Version of record

Article

Cell Reports

Inducible Degradation of the Human SMC5/6 Complex Reveals an Essential Role Only during Interphase

Graphical Abstract

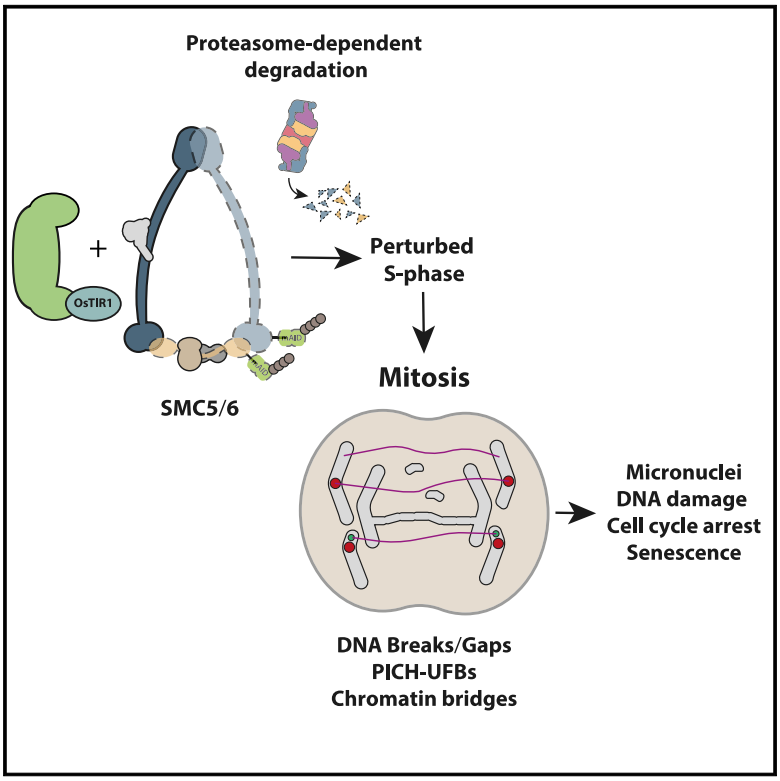

Highlights

- Subunits of the SMC5/6 complex are essential for mitotic growth in human cells
- Impaired SMC5/6 function is associated with increased mitotic aberrations
- SMC5/6 is required for proper disjunction of repetitive sequences in mitosis
- Mitotic defects following SMC5/6 loss are due to functions in interphase

Authors

Andrés Bueno Venegas, Toyoaki Natsume, Masato Kanemaki, Ian D. Hickson

Correspondence

iandh@sund.ku.dk

In Brief

Venegas et al. employ an auxin-inducible degron system for different subunits of the SMC5/6 complex to interrogate the short- and long-term effects of SMC5/6 impairment in human cells. Degradation of SMC5/6's subunits at different cell cycle stages places the essential role of the complex during S phase.

Venegas et al., 2020, Cell Reports *31*, 107533
April 21, 2020
https://doi.org/10.1016/j.celrep.2020.107533

CellPress

Cell Reports
Article

Inducible Degradation of the Human SMC5/6 Complex Reveals an Essential Role Only during Interphase

Andrés Bueno Venegas,[1] Toyoaki Natsume,[2,3] Masato Kanemaki,[2,3] and Ian D. Hickson[1,4,*]
[1]Center for Chromosome Stability and Center for Healthy Aging, Department of Cellular and Molecular Medicine, University of Copenhagen, Panum Institute, 2200 Copenhagen N, Denmark
[2]Division of Molecular Cell Engineering, National Institute of Genetics, Research Organization of Information and Systems (ROIS), Mishima, Shizuoka 411-8540, Japan
[3]Department of Genetics, SOKENDAI, Mishima, Shizuoka 411-8540, Japan
[4]Lead Contact
*Correspondence: iandh@sund.ku.dk
https://doi.org/10.1016/j.celrep.2020.107533

SUMMARY

The cohesin- and condensin-related SMC5/6 complex has largely been studied in the context of DNA repair. Nevertheless, SMC5/6 has an undefined essential function even in the absence of cellular stress. Through the use of an auxin-inducible degradation system for rapidly depleting subunits of the SMC5/6 complex, we show that SMC5/6 is essential for viability in cancer-derived and normal human cells. Impairment of SMC5/6 function is associated with spontaneous induction of DNA damage, p53 activation, cell-cycle arrest, and senescence, as well as an increased frequency of various mitotic chromosome segregation abnormalities. However, we show that this chromosome missegregation is apparent only when SMC5/6 function is impaired during the preceding S and G2 phases. In contrast, degradation of SMC5/6 immediately prior to mitotic entry has little or no impact on the fidelity of chromosome segregation, highlighting the importance of the complex during interphase in order to ensure faithful sister chromatid disjunction.

INTRODUCTION

Cell proliferation requires both the accurate duplication of the genome and the faithful segregation of the newly replicated sister genomes during mitosis. During these essential processes, the genome must undergo a series of dramatic structural changes that rely on the concerted action of numerous proteins. Among these proteins, members of the structural maintenance of chromosomes (SMC) family are involved in several processes that are important for the preservation of chromosome structure and integrity (Wu and Yu, 2012; Zhang et al., 2019). In eukaryotes, two SMC family members, cohesin (comprising SMC1–SMC3 and associated subunits) and condensin (comprising SMC2–SMC4 and associated subunits) have well-defined roles in chromosome organization, dynamics, and stability. In contrast, the third SMC family member, the SMC5/6 complex, is highly conserved in evolution, but its role is much less well defined (Aragón, 2018; Fernandez-Capetillo, 2016).

SMC5/6 is made up of two core SMC proteins, SMC5 and SMC6, as well as additional NSE (non-SMC element) subunits, which are critical for the stability and functions of the complex. Six NSEs (Nse1–6) are present in both budding and fission yeast. Although only four NSEs (NSE1–4) have been described thus far in human cells, the SLF2 (SMC5/6 localizing factor 2) protein was suggested recently to be a functional human ortholog of yeast Nse6 (Räschle et al., 2015). Some of the NSEs have defined catalytic roles: the heterodimer formed by NSE1/3 displays E3 ubiquitin ligase activity (Doyle et al., 2010), while the NSE2 subunit, which operates from its docking site on the coiled-coil region of SMC5, possesses a Siz/PIAS-RING domain that confers E3 SUMO ligase activity (Bermúdez-López et al., 2015; Duan et al., 2009; Potts and Yu, 2005). Interestingly, all of the subunits within the complex are essential for mitotic and meiotic growth in budding yeast, and inactivation of either Nse2 or Smc6 during early development is lethal in mice (Jacome et al., 2015; Ju et al., 2013).

Under unperturbed growth conditions, budding yeast *smc5/6* mutants accumulate X-shaped DNA structures that are believed to represent some type of joint DNA molecules (JMs) (Torres-Rosell et al., 2007). These structures are proposed to arise because of an inability to complete DNA replication at a subset of loci that are particularly susceptible to DNA replication perturbation. This "unfinished business" during replication leads to an accumulation of JMs that apparently escape detection by the G2/M DNA damage checkpoint and subsequently drives unbalanced segregation and/or mitotic catastrophe. Indeed, *smc5/6* mutants fail to efficiently segregate highly repetitive loci such as the rDNA cluster and telomeres (Torres-Rosell et al., 2005, 2007). In agreement with this, acute degradation of Smc5/6 subunits in budding yeast leads to replication defects specific to the rDNA during the first cell cycle (Peng et al., 2018). A second function of Smc5/6 has been proposed on the basis of the observation that following DNA damage or DNA replication stress, *smc5/6* mutants accumulate unresolved homologous recombination intermediates, highlighting a requirement for SMC5/6 in the resolution of DNA structures that arise during recombination-coupled DNA repair (Bermúdez-López et al., 2010; Pond et al., 2019).

Cells lacking a functional SMC5/6 complex display higher rates of sister chromatid exchanges (SCEs), a readout of crossing-over during homologous recombination repair (Kliszczak et al., 2012; Stephan et al., 2011). This is a phenotype that is characteristic of cells from individuals with Bloom's syndrome, which are deficient in the BLM helicase (Chu and Hickson, 2009). However, despite their overlapping roles, and the fact that Sgs1 (the budding yeast BLM ortholog) is SUMOylated by Smc5/6, BLM and the SMC5/6 complex appear to have largely independent roles (Bermúdez-López et al., 2016; Bonner et al., 2016). This contention is based on the fact that depletion of ySgs1/hBLM is non-epistatic with partial loss of Smc5/6 function and instead confers synthetic lethality/sickness (Chen et al., 2009; Menolfi et al., 2015; Räschle et al., 2015; Torres-Rosell et al., 2005).

In order to better understand how the SMC5/6 complex contributes to the maintenance of genomic stability in human cells, we have engineered a panel of human cell lines in which it is possible to inducibly degrade different subunits of the SMC5/6 complex. Our data indicate that SMC5/6 is essential for viability in both cancer-derived and non-cancerous immortalized cell lines. Loss of SMC5/6 function is associated with a greatly increased frequency of mitotic aberrations that fuel genomic instability, DNA damage, and ultimately cell death and senescence. We show that the mitotic abnormalities seen in cells with impaired SMC5/6 function are due to a function of the complex during interphase rather than during mitosis itself.

RESULTS

Development of a System to Inducibly Degrade the SMC5/6 Complex in Human Cell Lines

In budding and fission yeast, mutants lacking subunits of the Smc5/6 complex are not viable (Lehmann et al., 1995). Such mutants are able to proliferate for only a limited period of time but then arrest because of extensive chromosome abnormalities. In mammals, it is known that NSE2 and SMC6 (Jacome et al., 2015; Ju et al., 2013) are essential for embryonic development in mice, although it is not known whether SMC5/6 is essential for sustained cell proliferation in human cells. Therefore, we investigated whether acute depletion of different subunits of the human SMC5/6 complex had an effect on cell proliferation. To achieve this, we endogenously modified the genes encoding different components of the SMC5/6 complex in HCT116 cells such that they would express the targeted subunit fused to a minimal auxin-inducible degron (mAID) tag (Natsume et al., 2016). These cells also constitutively express a plant-derived E3 ubiquitin ligase, OsTIR1. In the presence of the plant hormone 3-indole-acetic acid (IAA), the interaction between OsTIR1 and mAID is strongly enhanced, resulting in the targeted degradation of the mAID-tagged protein. We observed that cells expressing NSE4A-mAID alone, or those expressing NSE4A-mAID together with SMC6-mAID, efficiently degraded the tagged subunits in response to IAA treatment (Figures 1A, 1B, S1A, and S1B). Moreover, and as shown previously for other subunits of the human SMC5/6 complex (Gallego-Paez et al., 2014; Potts and Yu, 2007), depletion of NSE4A alone (or in combination with SMC6) reduced the overall stability of the full complex, as evidenced by a gradual reduction in the total levels of untagged SMC5 (Figures 1B, S1A, and S1B). The same effect was observed in HCT116 expressing OsTIR1 under a doxycycline promoter and SMC6-mAID-Clover (SMC6-mAC) (Figures S1C and S1D). In support of the notion that simultaneous degradation of both NSE4A and SMC6 destabilized the complex to a greater extent than did degradation of either subunit alone, total levels of the untagged SMC5 subunit were 2-fold lower in the double-degron cells (Figure S1E). It should be noted that the levels of both NSE4A-mAID and SMC6-mAID were reduced in comparison with those in cells with untagged subunits, which we attribute to the ability of OsTIR1 to target mAID-tagged proteins for degradation even in the absence of IAA (Figure S1F). This contention was further supported by the fact that the levels of SMC6-mAC were strongly reduced upon doxycycline-driven expression of OsTIR1 (Figure S1D). We also analyzed whether degradation of SMC5/6 might indirectly influence the stability of other SMC proteins. As expected, there was no corresponding reduction in the cellular level of cohesin (SMC1/3) or condensin (SMC2/4) (Figure S1F).

Next, we tested whether SMC5/6 was important for continued proliferation in either human cancer cells (HCT116) or hTERT-immortalized non-cancer cells (RPE1). We observed that after 10 days of growth in the presence of 500 μM IAA, colony-forming ability was reduced dramatically (Figures 1C, 1D, and S1G–S1J). This effect was less pronounced in SMC6-mAC-expressing cells, which can be explained by the fact that not all cells in the population were able to degrade the protein, as confirmed by indirect immunofluorescence against Clover (Figures S1K–S1N). Importantly, IAA had little or no effect on the ability of the parental cells to form colonies (Figures S2A–S2D). Moreover, and as shown previously in both fission and budding yeast, we observed that cells lacking an active SMC5/6 complex were able to proliferate for two or three cell cycles, after which the growth rate declined rapidly (Figures 1E, S2E, and S2F; Lehmann et al., 1995). Therefore, we conclude that the SMC5/6 complex is essential for continued proliferation in transformed and untransformed human cells.

Impairment of SMC5/6 Function Is Associated with Increased DNA Damage, p53-p21 Activation, and Cell Senescence

SMC5/6 has been shown to be important for repair of DNA double-strand breaks (DSBs) (De Piccoli et al., 2006). We asked, therefore, whether the inability of cells to proliferate without a functional SMC5/6 complex might be due to an accumulation of unrepaired (and spontaneous) DNA damage. Consistent with this, levels of the CHK2 kinase phosphorylated at threonine-68 (CHK2-T68p; a marker of ATM kinase activation) were found to be increased upon acute co-depletion of NSE4A/SMC6 or SMC6 in HCT116 for 24 h (Figures 2A and S2G). This apparent accumulation of DNA damage was conserved and was not dependent on cellular transformation, as loss of SMC5/6 function in hTERT-RPE1 cells also generated high levels of CHK2-T68p (Figure S2H). Staining for the canonical DNA damage marker γH2A.X in cells treated with IAA for 4 days further confirmed that loss of SMC5/6 leads to a slight, but significant, increase in the levels of DNA damage in comparison

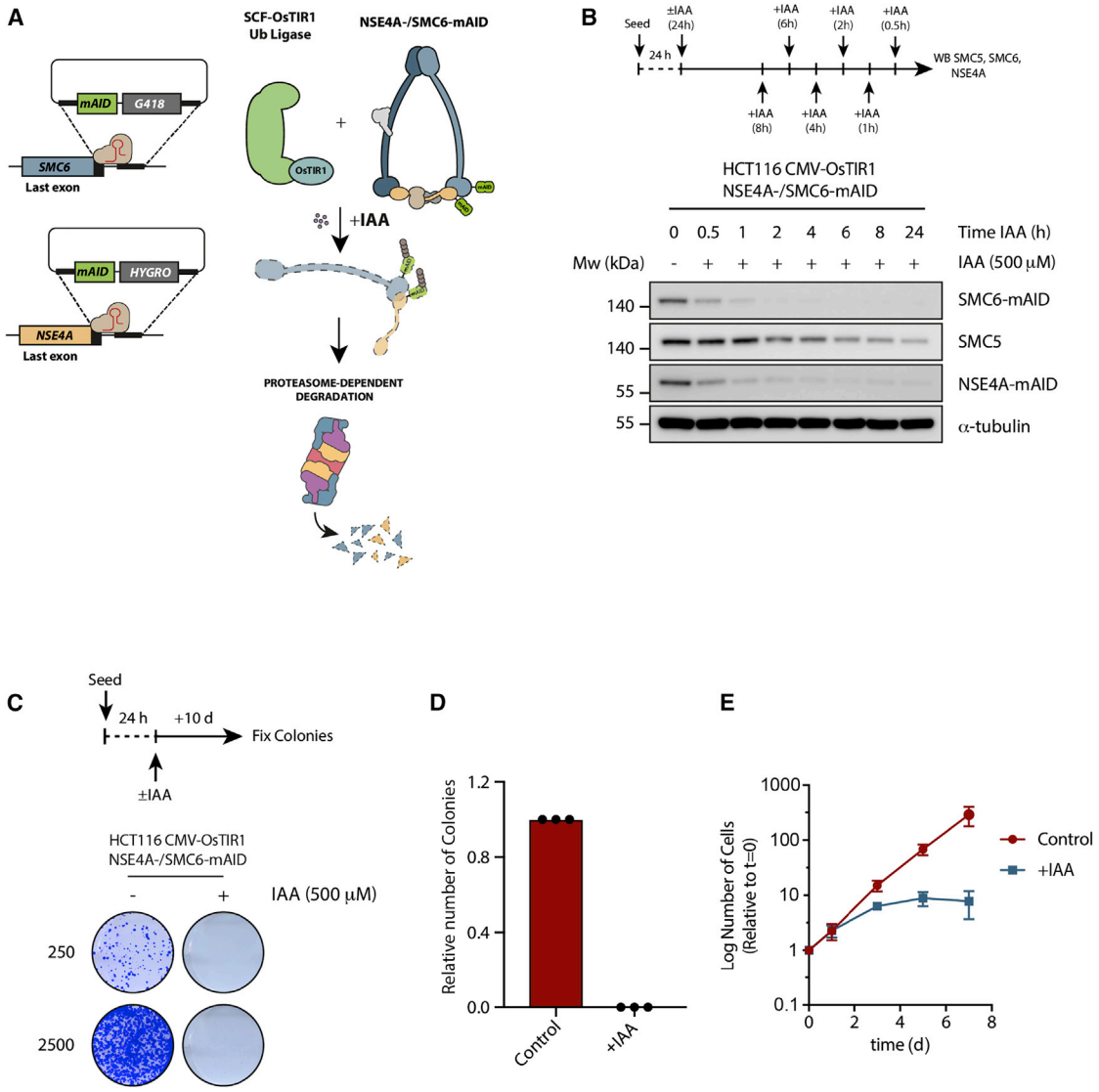

Figure 1. Subunits of the SMC5/6 Complex Are Essential in Human Colorectal Cancer Cells

(A) Outline of the strategy to endogenously tag both alleles of the NSE4A and SMC6 subunits with a minimal auxin-inducible degron (mAID).

(B) Top: protocol for assessing the timing of degradation of NSE4A and SMC6 upon addition of indole-acetic acid (IAA) to the medium. Bottom: asynchronously growing cells were treated or not with 500 μM IAA for different periods of time, and the levels of the indicated proteins were determined using western blotting. Note that the levels of SMC5, the other core component of the complex that is untagged, are also reduced upon auxin addition. α-Tubulin was used as a loading control.

(C) Colony formation assay of HCT116 NSE4A-/SMC6-mAID cells after a period of 10 days of growth in the absence or the presence of 500 μM IAA.

(D) Quantification of the number of colonies from (C) relative to control from three independent experiments.

(E) Time course of cell proliferation of HCT116 NSE4A-/SMC6-mAID cells after IAA addition. The number of cells was assessed every 2 days for a total period of 7 days. Points represent the mean ± SD of three independent experiments.

See also Figures S1 and S2.

with control cells (Figures 2B and 2C). However, levels of γH2A.X in NSE4A/SMC6-degraded cells were found to be much lower than those observed in cells treated with the DNA-damaging agent camptothecin, a topoisomerase I inhibitor (Figures 2B and 2C).

As persistent DNA damage can lead to cell-cycle arrest and senescence, we asked whether cells lacking a functional SMC5/6 complex might display altered levels of cell-cycle arrest markers. We observed that degradation of both NSE4A and SMC6 in HCT116 cells led to a concomitant increase in the expression of both p53 and p21, a phenomenon that was also observed in RPE1 cells depleted for SMC6 (Figures 2A and S2H). Moreover, and consistent with an increase in the expression of p53 and p21, those cells that remained viable after degradation of both

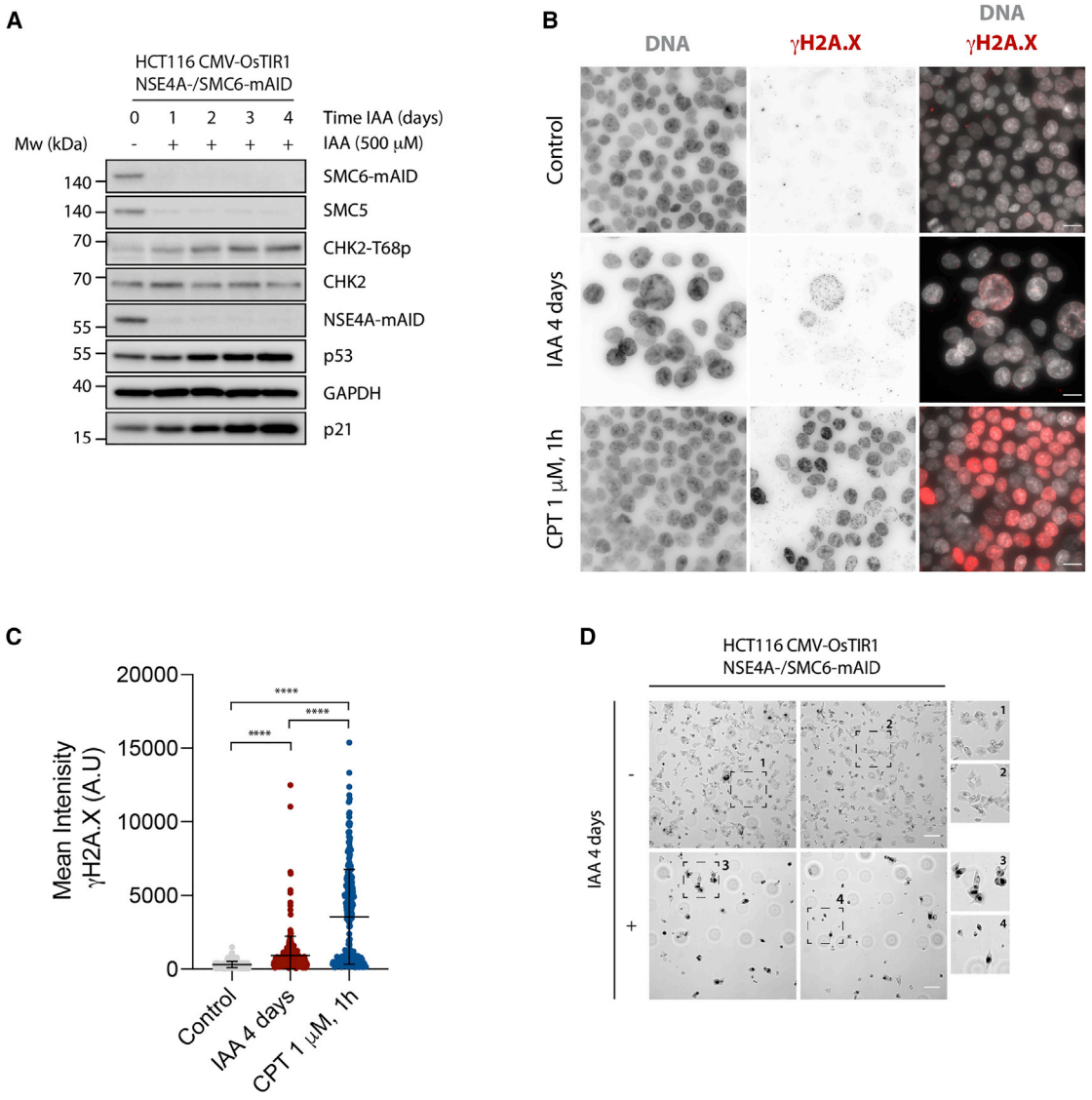

Figure 2. Loss of SMC5/6 Induces Mild DNA Damage

(A) Western blot showing the levels of different DNA damage and cell-cycle arrest markers upon NSE4A/SMC6 degradation for different lengths of time in HCT116 NSE4A/SMC6 cells. GAPDH was used as a loading control.

(B) Representative images showing levels of γH2A.X in control, cells degraded for NSE4A/SMC6 for 4 days, and cells treated with 1 μM camptothecin (CPT) for 1 h. Scale bar, 15 μm.

(C) Quantitation of γH2A.X levels of conditions shown in (B). More than 250 cells were quantified in total per condition from three independent experiments. Asterisks represent statistical analysis using an unpaired Student's t test (****$p < 0.0001$).

(D) After 4 days of growth in the absence or presence of IAA, cells were fixed and stained for β-galactosidase to assess cellular senescence, which is indicated by dark cytoplasmic staining. Scale bar, 10 μm.

See also Figure S3.

NSE4A/SMC6 for 4 days displayed staining for β-galactosidase, a widely used marker of cell senescence (Figure 2D). Hence, lack of a functional SMC5/6 appears to generate a persistent DNA damage response (DDR) that triggers the activation of the pro-apoptotic and pro-senescence p53-p21 axis.

We therefore considered whether this alone might be the cause of the loss of cell viability upon inactivation of SMC5/6. To test this, we inactivated *TP53* by CRISPR/Cas9-based gene targeting in HCT116 expressing both NSE4A-mAID and SMC6-mAID (Figures S3A and S3B). However, we observed that these p53-null cells still failed to form colonies following NSE4A and SMC6 degradation (Figures S3C and S3D), despite lacking upregulation of p21 (Figure S3E). Hence, we suggest that in the absence of a functional SMC5/6 complex, the p53-p21 axis is unlikely to be the only pathway for driving cell-cycle arrest, cell death, and senescence.

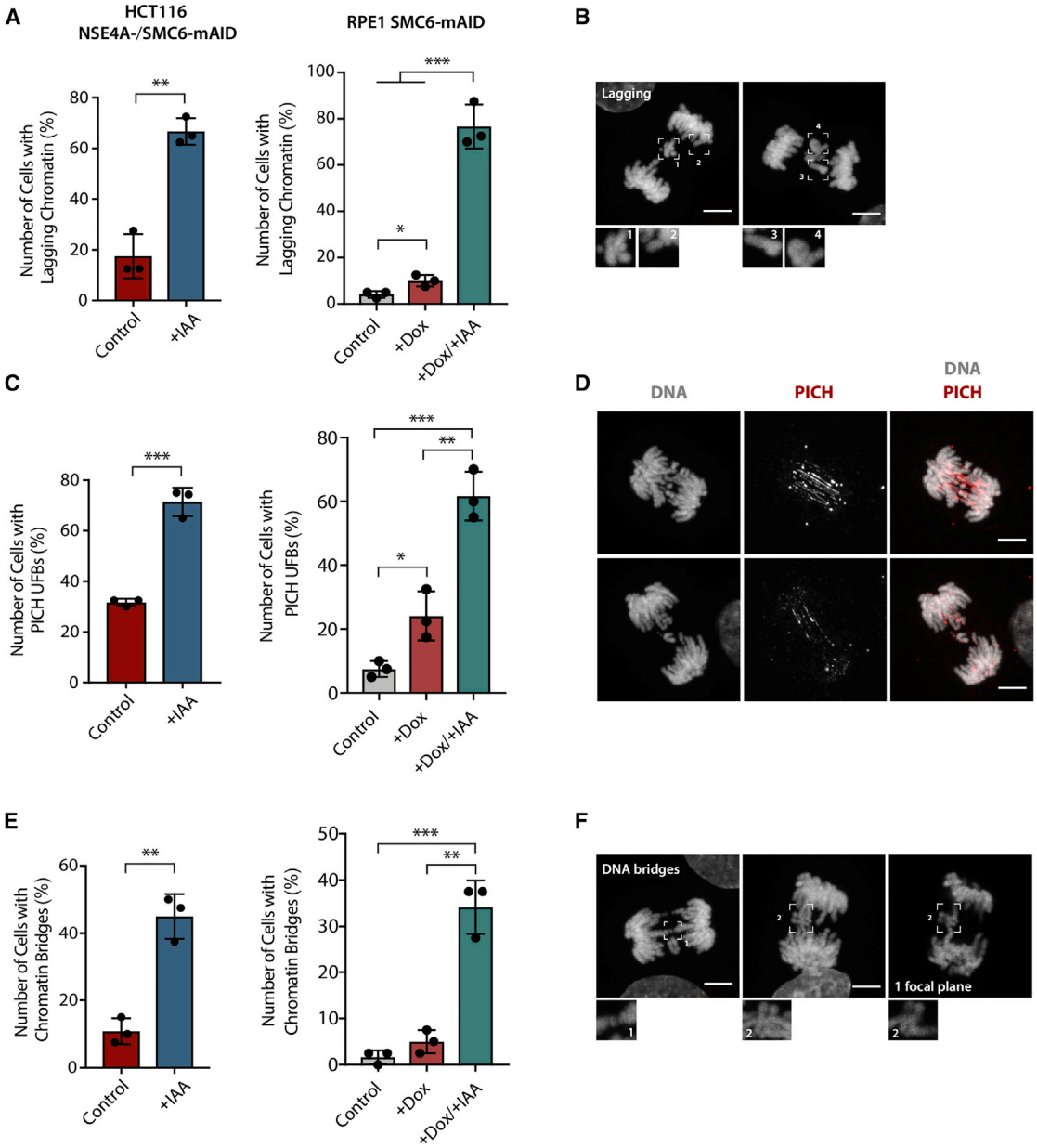

Figure 3. Loss of SMC5/6 Subunits Leads to Chromosome Missegregation

HCT116 NSE4A-/SMC6-mAID or hTERT-RPE1 SMC6-mAID cells were grown for 24 h in the absence or presence of IAA. Anaphase cells were then analyzed for the presence of different mitotic aberrations.

(A–F) Quantification (left) and representative anaphases (right) of cells displaying (A and B) lagging chromatin, (C and D) PICH-coated UFBs, or (E and F) chromatin bridges. For each quantification, HCT116 cells are shown on the left and RPE cells on the right.

Mean values are shown ± SD. Error bars indicate mean ± SD of three independent experiments (120 cells were analyzed in total in each condition; 40 cells/experiment). Asterisks represent statistical analysis using an unpaired Student's t test (**$p < 0.01$, ***$p < 0.001$, and ****$p < 0.0001$).

SMC5/6 Ensures Faithful Chromosome Segregation in Human Cells

We next sought to identify the causes of the terminal phenotype observed upon SMC5/6 degradation. SMC5/6 has been shown to be important for accurate chromosome segregation in different organisms, including yeast and humans (Behlke-Steinert et al., 2009; Gallego-Paez et al., 2014; Payne et al., 2014). We asked, therefore, whether the terminal phenotype seen in our SMC5/6 degron system was preceded by chromosome missegregation and/or other mitotic abnormalities during mitosis. Degradation of both NSE4A and SMC6 in HCT116 cells, or of SMC6 alone in RPE1 cells, for 24 h led to a significant increase in the number of cells displaying mitotic errors during anaphase (Figure 3). The fraction of cells displaying either lagging

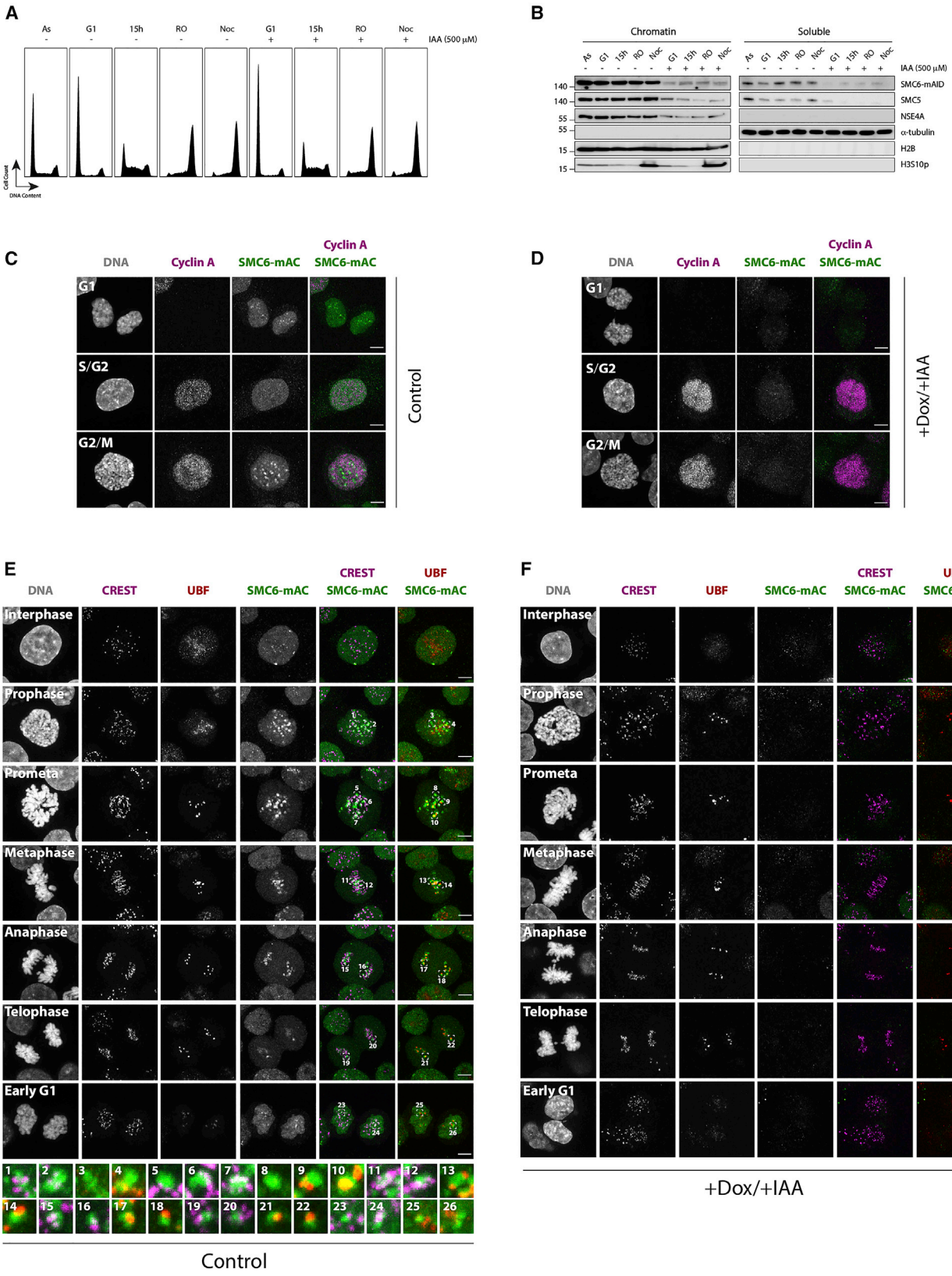

(legend on next page)

chromatin between the two segregating DNA masses in anaphase or ultrafine DNA bridges (UFBs) coated with PICH (defining double-stranded DNA [dsDNA]) was increased about 3-fold (Figures 3A–3D). The frequency of bulky DNA bridges was also increased (approximately 2-fold) in cells with impaired SMC5/6 function (Figures 3E and 3F). Therefore, degradation of human SMC5/6 components during a single cell cycle in the absence of additional cellular stress leads to mitotic aberrations that might be acting as the trigger of the terminal phenotype observed in cells with impaired SMC5/6 function. We address this issue in more detail below.

SMC5/6 Redistributes to Specific Nuclear Regions during Mitosis

It has been shown previously that SMC5/6 associates less prominently with chromatin after cells enter mitosis (Lindroos et al., 2006; Gallego-Paez et al., 2014). To investigate the origin of the anaphase segregation defects following SMC5/6 degradation, we first assessed the levels of different subunits of the SMC5/6 complex (SMC5, SMC6, and NSE4A) in the chromatin fraction at different cell cycle stages. In order to obtain a highly synchronized cell population, we arrested HCT116 NSE4A-/SMC6-mAID cells with lovastatin, a cholesterol synthesis inhibitor that arrests cells in G1. Cells were then released from the G1 block, and samples were taken at different time points (Figure 4). Where required, cells were then either arrested in late G2 with the CDK1 inhibitor RO-3306 or in prometaphase with nocodazole (Figure 4A). All of the SMC5/6 complex subunits analyzed were found to be associated with the chromatin fraction from G1 to mitosis (Figure 4B). In addition, levels of NSE4A-mAID, SMC6-mAID, and untagged SMC5 remained largely constant throughout the cell cycle. As expected, cells degraded for both NSE4A and SMC6 during G1 showed highly reduced levels of both subunits on chromatin. A similar effect could also be observed for SMC5 (Figure 4B).

To confirm that the recruitment of different subunits of the complex to chromatin was not affected by the mAID-tag used, we followed the recruitment pattern of untagged SMC6 in wild-type HCT116 cells at different times after a G1 release. In agreement with what we observed in HCT116 NSE4A-/SMC6-mAID cells, SMC6 was present on chromatin from G1 until mitosis, and its association with chromatin remained similar at the different cell cycle stages analyzed (Figures S4A and S4B). Hence, at least in HCT116 cells, SMC5/6 can be found on chromatin throughout the cell cycle and does not appear to be eliminated from chromatin in mitosis.

We next sought to define the subcellular localization pattern of SMC5/6 during the different cell cycle phases. For this, we used HCT116 Tet-OsTIR1 SMC6-mAC cells, in which SMC6 was endogenously tagged with mAID-Clover. In G1 and S/G2 cells, identified as being negative and positive for cyclin A, respectively, SMC6-mAC was distributed generally throughout the nucleus (Figures 4C and 4E). As cells approached mitosis, SMC6-mAC started to localize more distinctly and then redistributed to specific chromatin regions during mitosis (Figure 4E). To analyze whether SMC5/6 might localize to centromeres during mitosis, we studied its co-localization with the centromeric marker CREST. Strikingly, SMC6-mAC often co-localized with CREST in mitotic cells, although it appeared to be more strongly enriched on certain chromosomes. As SMC5/6 was previously found to be important for the accurate segregation of the rDNA in yeast, we analyzed whether SMC6-mAC was enriched at the rDNA repeat regions found on the short arms of the five acrocentric chromosomes (13, 14, 15, 21, and 22). Using UBF as an rDNA marker, we observed that SMC6-mAC was highly enriched around rDNA repeats during all stages of mitosis (Figure 4E). This observation was further confirmed by analyzing the localization of SMC6-mAC on chromosome spreads. Counterstaining of chromosome spreads with CREST, UBF, and GFP showed a clear enrichment of SMC6-mAC around the rDNA loci and, to a lesser extent, to all centromeric regions on all chromosomes (Figures S4C and S4D). Consistently, the signal detected by indirect immunofluorescence against SMC6-mAC disappeared upon degradation of the protein for 24 h (Figures 4D and 4F), confirming the specificity of the antibody.

Degradation of SMC5/6 Subunits during G1, but Not Prior Entry into Mitosis, Affects Chromosome Segregation

Given the pattern of localization of SMC5/6 during mitosis, we next investigated whether the mitotic aberrations seen following SMC5/6 degradation might be due to a specific function of the complex during mitosis. To address this, we exploited the ability of our system to rapidly degrade both NSE4A and SMC6 in HCT116 cells arrested at different stages of the cell cycle (Figures 5A, S5A, and S5B). Surprisingly, given the defined localization pattern for the SMC5/6 complex in mitosis, we observed that degradation of NSE4A and SMC6 during late G2 phase did not increase the frequency of mitotic aberrations. In contrast, degradation prior to S-phase entry gave rise to a significant increase in the number of cells displaying mitotic aberrations (Figures 5B–5H and S5C).

Figure 4. Localization of Subunits of the SMC5/6 Complex throughout the Cell Cycle

(A) FACS profiles of HCT116 NSE4A-/SMC6-mAID cells at different cell cycle stages (asynchronous [As], G1 arrested [G1], S phase [15 h], G2 [RO], and mitosis [Noc]).

(B) Western blot showing recruitment to chromatin of SMC6-mAID, SMC5, and NSE4A-mAID in the absence or presence of IAA at different cell cycle stages. Labeling as in (A). α-Tubulin and histone H2B were used as loading controls for the soluble and chromatin-associated fractions, respectively. Histone H3S10p was used as a mitotic marker for cells arrested in nocodazole.

(C and D) SMC6-mAC is recruited to the nucleus in G1-, S/G2-, and G2/M-phase cells in the absence of auxin (C) and is degraded after auxin addition (D). Cyclin A was used as a marker for S/G2 phases. Note that cyclin A is absent from G1 cells.

(E and F) HCT116 Tet-OsTIR1 SMC6-mAC were grown in the absence (E) or presence (F) of 100 ng/mL doxycycline and 500 μM IAA for 24 h, and the localization of SMC6 throughout mitosis was monitored by indirect immunofluorescence using an anti-GFP antibody. CREST was used as a centromeric marker, and UBF was used as an rDNA marker. Scale bars, 5 μm.

See also Figure S4.

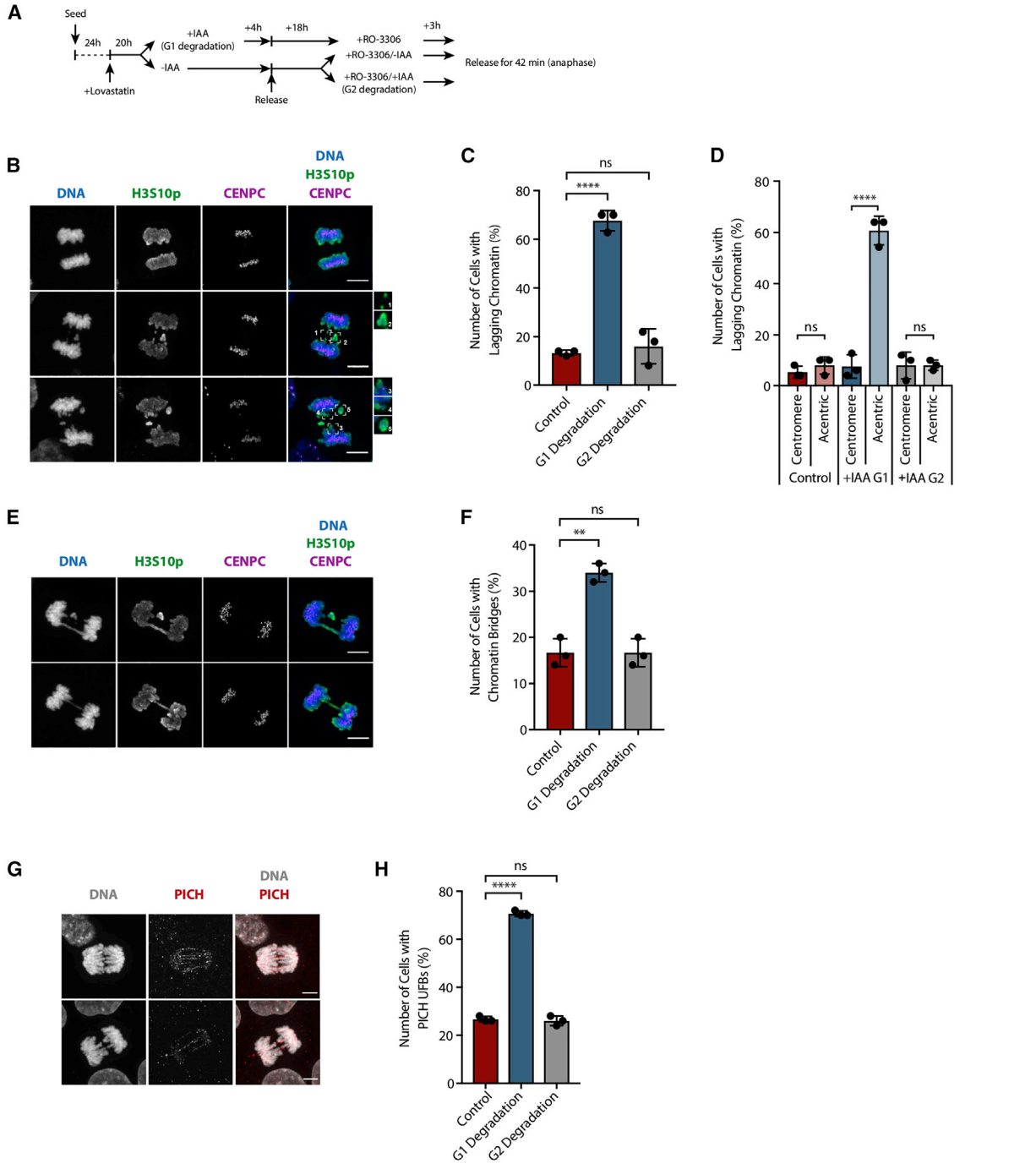

Figure 5. SMC5/6 Deficiency during S Phase Affects Mitotic Chromosome Segregation

(A) Experimental workflow for assessing mitotic aberrations during anaphase upon degradation of NSE4A and SMC6 either in G1 or immediately before mitosis.

(B) Representative images of cells displaying lagging chromatin that is either positive or negative for centromeres, marked using an anti-CENPC antibody. H3S10p staining was used to assist in the identification of smaller fragments of condensed chromatin that were not always visible by DAPI staining.

(C and D) Quantification of the percentage of anaphase cells displaying lagging chromatin (C) and whether the lagging chromatin was acentric or not (D).

(E and F) Representative images of anaphase cells showing chromatin DNA bridges (E) and quantification of the percentage of cells displaying chromatin DNA bridges (F).

(legend continued on next page)

SMC5/6 Degradation Increases UFBs Arising from Repetitive Sequences

The SMC5/6 complex has been studied extensively for its role in ensuring proper segregation of the rDNA locus in budding yeast (Torres-Rosell et al., 2005). We therefore analyzed whether the UFBs coated by PICH observed in cells lacking a functional SMC5/6 might originate from rDNA loci or perhaps other highly repetitive regions (Figures S5D and S5E). We observed that impairment of SMC5/6's function prior to entry into S phase led to a significant increase in cells displaying PICH-coated UFBs arising not only from the rDNA but also from centromeres. Consistent with a lack of a role for SMC5/6 in mitosis itself, the frequency of rDNA and centromeric UFBs was not elevated in cells in which SMC5/6 was degraded just prior to the G2/M transition (Figure S5D). It should be noted that most anaphase cells that went through S phase in the absence of a functional SMC5/6 complex also displayed a class of PICH UFBs that were negative for both centromeric and rDNA markers (Figures S5D and S5E).

Inhibition of TOP2α with catalytic inhibitors such as ICRF-193 leads to an accumulation of chromatin bridges and PICH-coated UFBs arising from centromeres, a phenotype that resembles what we have observed in cells lacking a functional SMC5/6 complex. Recently, it has also been shown that both TOP2α and the SMC5/6 complex interact in human cells and that NSE2-dependent SUMOylation of TOP2α is important for accurate chromosome segregation (Deiss et al., 2019). In agreement with this proposed functional interaction between TOP2α and SMC5/6, we observed that NSE4A-/SMC6-degraded cells displayed an increased level of sensitivity to low doses of ICRF-193, as evidenced by an increase in both the frequency of anaphase cells displaying PICH-coated UFBs and number of PICH UFBs displayed per anaphase cell (Figures S5F–S5H).

Mitotic chromosomes of cells depleted for different SMC5/6 subunits have been shown to display either a reduction in the levels of TOP2α or an alteration in its distribution pattern (Deiss et al., 2019; Gallego-Paez et al., 2014). To test whether the appearance of PICH UFBs arising from centromeres and the rDNA in NSE4A-/SMC6-degraded cells is related to a defect in the recruitment or retention of TOP2α on chromatin, we assessed for the levels of TOP2α on mitotic chromosomes of HCT116 cells degraded for both NSE4A and SMC6 for 24 h. The chromatin-associated fraction of TOP2α in nocodazole-arrested cells did not show any significant alterations between control and degron cells (Figures S6A–S6C). Moreover, analysis of the distribution of TOP2α on chromosome spreads did not reveal any obvious abnormality (Figure S6D).

SMC5/6-Depleted Cells Display Higher Levels of Chromosome Fragmentation, Fragility, and Micronucleation

In order to investigate the origin of the mitotic problems in cells depleted for NSE4A/SMC6 during G1, we assessed whether the lagging chromatin observed in anaphase was positive for centromere-associated kinetochore factors. Interestingly, the lagging chromatin in the vast majority of cells was CENPC negative, indicative of an absence of centromeric DNA (Figures 5B–5D). As this phenomenon might be due to increased chromosome fragility, we asked whether mitotic chromosomes of cells depleted for NSE4A and SMC6 in G1 showed an increased frequency of breaks or gaps. Indeed, we observed an accumulation of breaks/gaps on metaphase chromosomes when the function of the SMC5/6 complex was impaired prior to S-phase entry, but not when it was compromised just prior to mitosis (Figures 6A–6D). Strikingly, although most of the breaks/gaps found in control and in G2-degraded cells were evident on only one sister chromatid, as is typical for common fragile site (CFS)-associated breakage (Bhowmick et al., 2016; Minocherhomji et al., 2015), approximately 50% of the breaks in SMC5/6 depleted cells involved both chromatids when SMC5/6 was degraded in G1 (Figure 6E).

We next asked whether the abnormalities observed during mitosis following NSE4A/SMC6 degradation were transmitted to the next generation of daughter cells. To this end, cells depleted for NSE4A/SMC6 either during G1 or prior to entry into mitosis were released from a G2 block for 2 h in the presence of a concentration of cytochalasin B that generated cytokinesis-blocked, pseudo-G1 cells (Figure 7A). We observed that these daughter cells displayed a significantly increased frequency of micronuclei only when SMC5/6 was degraded in G1 (Figures 7B–7D).

SMC5/6 Is Not Required for Bulk DNA Replication

The phenotype displayed by cells with impaired SMC5/6 complex function during S phase closely resembles that observed in cells exposed to a low dose of the DNA polymerase inhibitor aphidicolin. In order to test whether the chromosome fragility associated with SMC5/6 complex degradation was a direct consequence of delayed DNA replication, we first tested whether NSE4A/SMC6-depleted cells progressed through S phase with the same kinetics as control cells. As shown by propidium iodide fluorescence-activated cell sorting (PI-FACS), cells with impaired SMC5/6 function progressed through S phase with normal kinetics (Figures S7A and S7B). Moreover, analysis of the phosphorylation status of the transcription factor FoxM1 after G1 release did not show any evidence of premature entry into mitosis, as is observed, for example, when ATR is inhibited (Figure S7C; Saldivar et al., 2018). To further confirm that SMC5/6 did not have an impact on bulk DNA replication, we analyzed the speed of individual replication forks in unperturbed conditions using DNA fiber analysis. We observed that the mean fork speed in control and NSE4A/SMC6-degraded cells was very similar (Figures S7D–S7F).

In fission yeast, *smc5/6* mutants have been shown to be able to activate the DNA damage checkpoint efficiently, although they fail to maintain the activity of this checkpoint when the damage is removed. As a result, these mutant cells enter mitosis with unrepaired DNA damage that poses a problem for accurate chromosome segregation (Harvey et al., 2004). As discussed above, we consistently observed that HCT116 cells degraded for both

(G and H) Representative images of anaphase cells displaying PICH-coated UFBs (G) and quantification of number of anaphase cells containing these UFBs (H) under control conditions or following SMC5/6 degradation in G1 or G2.

Mean values are shown ± SD. Error bars indicate mean ± SD of three independent experiments (120 cells were analyzed in total in each condition; 40 cells/experiment). Asterisks represent statistical analysis using an unpaired Student's t test (**$p < 0.01$, ***$p < 0.001$, and ****$p < 0.0001$). Scale bars, 5 μm. See also Figure S5.

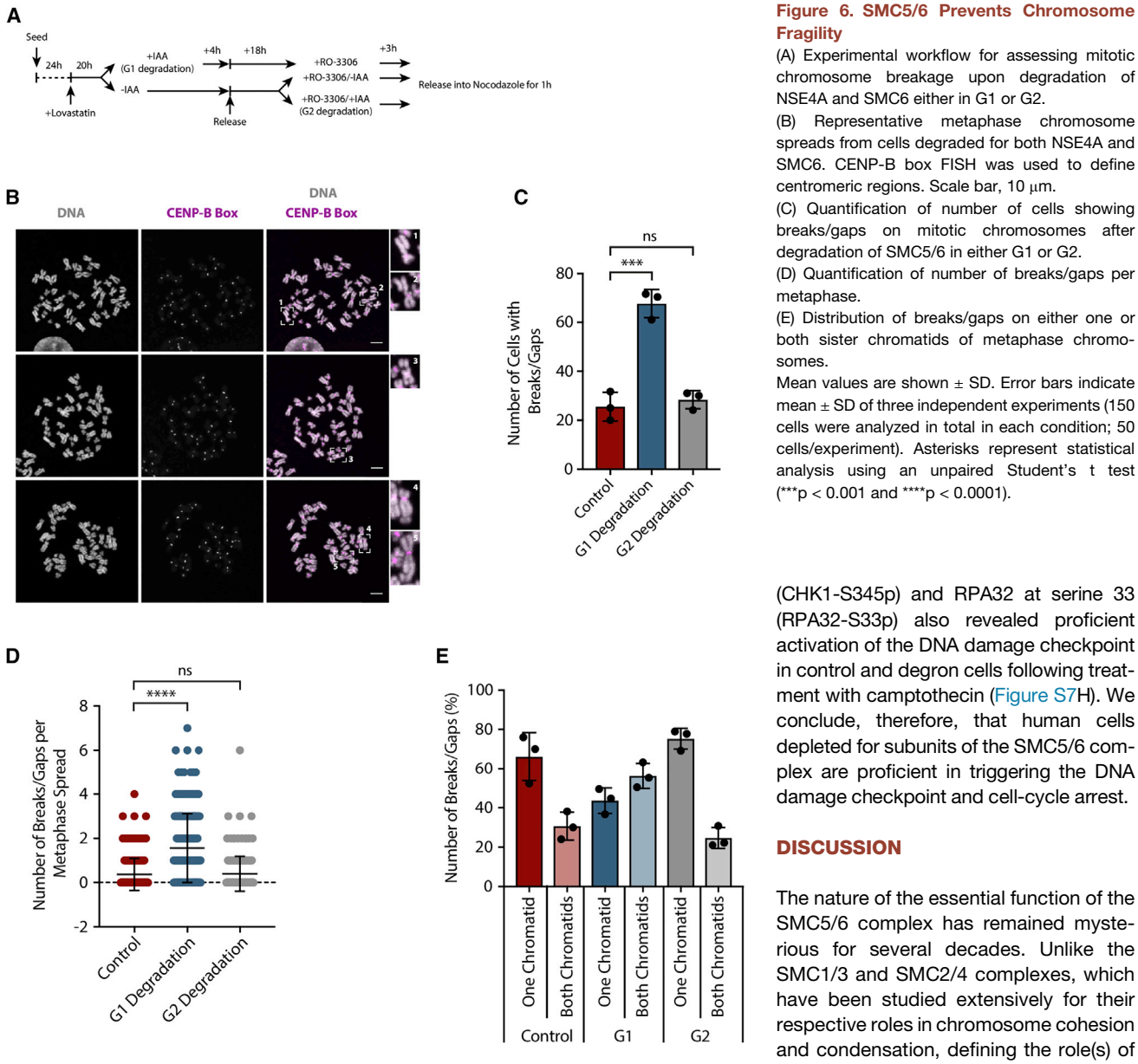

Figure 6. SMC5/6 Prevents Chromosome Fragility

(A) Experimental workflow for assessing mitotic chromosome breakage upon degradation of NSE4A and SMC6 either in G1 or G2.

(B) Representative metaphase chromosome spreads from cells degraded for both NSE4A and SMC6. CENP-B box FISH was used to define centromeric regions. Scale bar, 10 μm.

(C) Quantification of number of cells showing breaks/gaps on mitotic chromosomes after degradation of SMC5/6 in either G1 or G2.

(D) Quantification of number of breaks/gaps per metaphase.

(E) Distribution of breaks/gaps on either one or both sister chromatids of metaphase chromosomes.

Mean values are shown ± SD. Error bars indicate mean ± SD of three independent experiments (150 cells were analyzed in total in each condition; 50 cells/experiment). Asterisks represent statistical analysis using an unpaired Student's t test (***$p < 0.001$ and ****$p < 0.0001$).

NSE4A and SMC6 in G1 do not experience any delay in the cell cycle, suggesting that lack of a functional SMC5/6 complex during a single cell cycle does not lead to a level of DNA damage that is sufficient to activate the DNA damage checkpoint. However, another possible explanation for this is that SMC5/6 deficient cells are unable to activate the checkpoint in the first place. To address whether loss of SMC5/6 impairs checkpoint activation, we treated control and NSE4A-/SMC6-degraded cells with low doses of camptothecin upon release from lovastatin and followed their progression through the cell cycle using PI-FACS (Figure S7G). We found that both control and NSE4A-/SMC6-degraded cells progressed through S phase with the same kinetics in the presence of camptothecin and then became arrested at the G2/M boundary, indicative of activation of the DNA damage checkpoint in both cases. Monitoring of CHK1 phosphorylated at serine 345 (CHK1-S345p) and RPA32 at serine 33 (RPA32-S33p) also revealed proficient activation of the DNA damage checkpoint in control and degron cells following treatment with camptothecin (Figure S7H). We conclude, therefore, that human cells depleted for subunits of the SMC5/6 complex are proficient in triggering the DNA damage checkpoint and cell-cycle arrest.

DISCUSSION

The nature of the essential function of the SMC5/6 complex has remained mysterious for several decades. Unlike the SMC1/3 and SMC2/4 complexes, which have been studied extensively for their respective roles in chromosome cohesion and condensation, defining the role(s) of the SMC5/6 complex during DNA metabolism has proved more challenging. This may be because SMC5/6 is both a structural SMC protein and an enzyme that post-translationally modifies other proteins via its E3 SUMO ligase and E3 ubiquitin ligase activities. Hence, SMC5/6 may play a more diverse role during DNA metabolism than either cohesin or condensin.

In this study, we generated a panel of cell lines in which different subunits of the SMC5/6 complex could be degraded rapidly by addition of IAA to the culture medium. This allowed us to study not only the short-term but also the long-term effects of impairing SMC5/6 function. We have shown that degradation of either NSE4A or SMC6 destabilizes the whole SMC5/6 complex and that this abrogates cell growth in both HCT116 human colorectal cancer cells and hTERT-RPE1 non-cancer cells. In both cases, these cells are able to

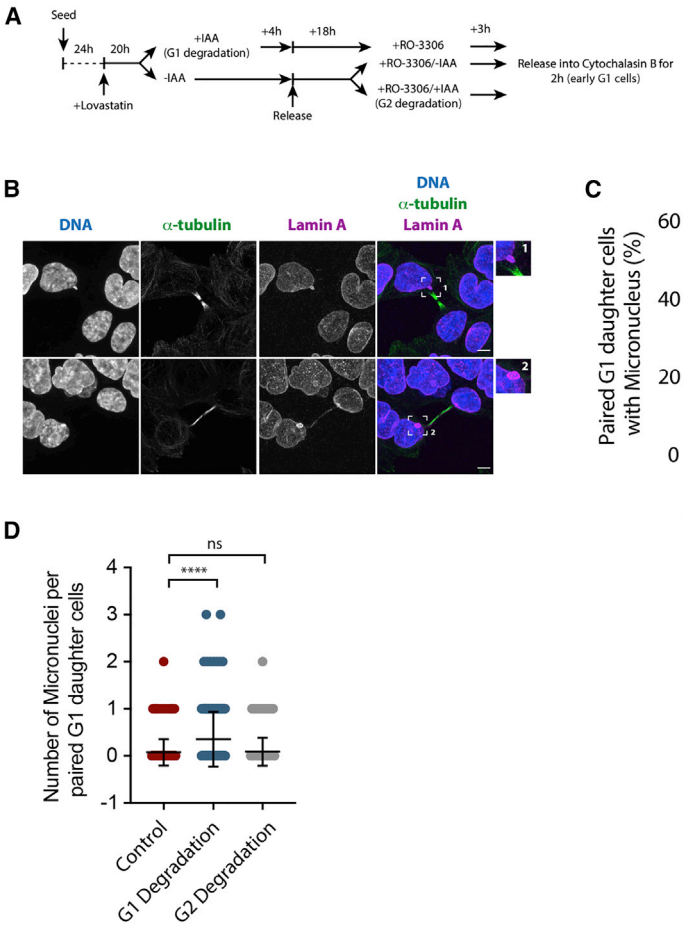

Figure 7. Consequences of Loss of SMC5/6 in the Following G1 Phase

(A) Experimental workflow for assessing the frequency of micronuclei in the following G1 phase after degradation of NSE4A-/SMC6-mAID before S phase or before mitosis in the preceding cell cycle.

(B) Representative images of G1 daughter cells displaying micronuclei of cells that have been degraded for NSE4A/SMC6 during G1. α-Tubulin was used to identify early G1 cells that were still connected after cytochalasin B treatment. Lamin A was used to show that cells had reformed the nuclear membrane in G1.

(C) Quantification of early G1 daughter cells containing at least one micronucleus.

(D) Quantification of the number of micronuclei displayed per G1 daughter cell.

Mean values are shown ± SD. Error bars indicate mean ± SD of three independent experiments (120 cells were analyzed in total; 40 cells/experiment). Asterisks represent statistical analysis using an unpaired Student's t test (****$p < 0.0001$).

proliferate for two or three cell generations, after which they cease dividing, consistent with what has previously been seen in budding and fission yeast *smc5/6* mutants (Lehmann et al., 1995). Degradation of the human SMC5/6 complex was accompanied by an accumulation of DNA damage and activation of p53. Nevertheless, inactivation of the *TP53* gene did not rescue the lethality observed in the absence of a functional SMC5/6. Therefore, this failure to rescue lethality indicates that a pathway other than the p53-p21 axis must be involved in triggering loss of proliferative capacity. Considering that lack of a functional SMC5/6 leads to an increase in the frequency of cells with micronuclei in the ensuing G1 phase, it is conceivable that the cGAS-STING pathway triggers cell-cycle arrest and senescence in cells with impaired SMC5/6 function (Glück et al., 2017). Further work will be required to address this possibility.

One of the key questions we aimed to address by the use of a degron system was to define the stage of the cell cycle during which SMC5/6 function is particularly required. We have shown that subunits of the SMC5/6 can already be found on chromatin in G1-arrested cells and that all subunits tested (NSE4A, SMC5, and SMC6) are present on chromatin during S phase, G2, and mitosis. In addition, and contrary to what was shown previously in human non-transformed hTERT-RPE1 cells (Gallego-Paez et al., 2014), we observed that SMC5/6 redistributes to mitotic chromatin around centromeres and the rDNA loci following nuclear envelope breakdown (NEBD). This discrepancy might be explained by differences in the cellular background or the approach used to detect SMC5/6 in cells. Whereas Gallego-Paez et al. (2014) combined indirect immunofluorescence against SMC5 with live cell imaging using SMC5-EGFP, we have assessed the localization of SMC5/6 throughout the cell cycle by using SMC6 endogenously tagged with mAID-Clover.

Mutation or depletion of subunits of the SMC5/6 complex is associated with increased genomic instability seen during or after mitosis in many eukaryotic cell types (Jacome et al., 2015; Payne et al., 2014; Torres-Rosell et al., 2007; van der Crabben et al., 2016). Here, we have shown that acute inactivation of SMC5/6 via degradation of both NSE4A and SMC6 in HCT116 cells or of SMC6 in hTERT-RPE1 cells has dramatic consequences during mitosis, with increased levels of lagging chromatin, bulky DNA bridges, and PICH-coated UFBs after degradation of mentioned subunits for as little as 24 h. Nevertheless, by exploiting the ability to effect rapid degradation of SMC5/6 upon auxin addition, we have interrogated whether the phenotype observed during mitosis is due to a role of the complex during interphase or mitosis. Surprisingly, the mitotic phenotype is observed only when the function of the complex is impaired prior to S-phase entry and not when it is impaired in late G2, indicating that the mitotic problems observed are a consequence of lack of SMC5/6 during the S/G2 phases rather than during mitosis. Furthermore, lack of SMC5/6 leads to an increase in PICH UFBs arising from centromeres and the rDNA, which supports the idea that SMC5/6 is not only enriched at these highly repetitive regions but also is required for the removal

of a subset of unresolved DNA intertwinings. In agreement with a role for SMC5/6 in facilitating disjunction of centromeric DNA, it has been shown recently that TOP2α, the major enzyme required for centromeric DNA decatenation, is SUMOylated by NSE2 and that this process is important for proper chromosome segregation (Deiss et al., 2019).

However, impairment of SMC5/6 functions leads to an increase in PICH-coated UFBs even in cells in which TOP2α is inhibited, suggesting that although some crosstalk likely exists between SMC5/6 and TOP2α, these proteins also act at least partially independently in order to ensure accurate chromosome segregation.

We have shown that SMC5/6 impairment for one cell cycle does not lead to decreased levels of TOP2α on chromatin or to a change in its recruitment pattern along the chromosome scaffold, as suggested previously (Deiss et al., 2019; Gallego-Paez et al., 2014). This discrepancy can be explained by differences in the time the cells have been dividing in absence of a functional SMC5/6. While we have been assessing the immediate effects of impairing the complex's function, Gallego-Paez et al. (2014) and Deiss et al. (2019) looked at long-term effects (e.g., two or three cell cycles after depletion of subunits with small interfering RNAs [siRNAs]). It is therefore possible that both the aberrant distribution of TOP2α along the chromosome arms and its complete absence is due to an accumulation of problems upon SMC5/6 loss rather than to a direct consequence of the degradation of subunits of the complex.

In addition, our data are in agreement with the observation that yeast Smc5/6 is highly enriched at the rDNA locus and that it is essential for the completion of replication of the rDNA, thus facilitating rDNA segregation during anaphase (Peng et al., 2018; Torres-Rosell et al., 2005). However, even though SMC5/6 has a very defined pattern of localization around the rDNA during mitosis, we did not observe any obvious mitotic phenotype that specifically involved the acrocentric chromosomes upon degradation of both NSE4A and SMC6 during G2. This suggests that rDNA segregation per se does not rely on a specific function of the SMC5/6 complex during mitosis itself. However, it cannot be ruled out that the enrichment of SMC5/6 around the rDNA repeats during mitosis reflects a function of the complex in a process other than decatenation, such as the modulation of transcription of these loci during mitosis and/or during the ensuing G1 phase.

NSE4A/SMC6-degraded cells display increased "spontaneous" chromosome fragility, as shown by a higher frequency of breaks/gaps on mitotic chromosomes and of chromosome fragments negative for centromeric markers in anaphase. This fragility phenotype resembles that of cells undergoing mild replication stress, such as exposure to a low dose of the DNA polymerase inhibitor aphidicolin. However, cells with impaired SMC5/6 function do not show any delay in progression through the cell cycle following G1 release, unlike aphidicolin-treated cells. This is in agreement with what has been recently shown upon acute co-depletion of both Smc6 and Nse5 during a G1 arrest in budding yeast and supports the notion that lack of functional SMC5/6 is not required for bulk DNA replication (Peng et al., 2018). Nevertheless, this does not rule out the possibility that SMC5/6 might be important for completion of replication at a small number of specific loci such as the rDNA (Peng et al., 2018; Torres-Rosell et al., 2005). Our observation that SMC5/6 is not essential for bulk DNA replication differs from that reported previously in hTERT-RPE1 cells, in which a marked delay in S phase was observed (Gallego-Paez et al., 2014). Again, this apparent contradiction could be due to differences between the cellular backgrounds used in the different studies or to differences in the experimental conditions used to synchronize and degrade different subunits of SMC5/6. Whereas Gallego-Paez et al. (2014) followed cell cycle progression after a G0 release in cells depleted for SMC5 or SMC6 by using siRNAs, we have used lovastatin combined with IAA-induced degradation of NSE4A and SMC6.

If SMC5/6 were important for releasing torsional stress behind replication forks, as it has been suggested (Kegel et al., 2011), it would be predicted that NSE4A/SMC6-deficient cells would be more prone to accumulate catenated sister chromatids following DNA replication. Moreover, the accumulation of torsional stress ahead of the advancing replication fork could be an impediment for the replisome, which might increase the likelihood of conflicts between the replication and transcription machineries and the accumulation of R-loops. In support of this notion, budding yeast expressing a thermosensitive allele for *nse4* display increased levels of R-loops (Chang et al., 2019). It is therefore possible that the lack of a functional SMC5/6 complex during S phase in human cells could lead to an accumulation of toxic levels of R-loops and a concomitant increase in conflicts between the replication and transcription machineries. Future studies should be aimed at addressing the validity of this proposal.

STAR★METHODS

Detailed methods are provided in the online version of this paper and include the following:

- KEY RESOURCES TABLE
- RESOURCE AVAILABILITY
  - Lead Contact
  - Materials Availability
  - Data and Code Availability
- EXPERIMENTAL MODEL AND SUBJECT DETAILS
- METHOD DETAILS
  - Colony formation assays
  - Cell synchronization
  - Chromosome spreads and centromeric FISH
  - Cell cycle analysis
  - Preparation of protein extracts and western blotting
  - Chromatin fractionation
  - DNA fibers
  - Immunofluorescence
- QUANTIFICATION AND STATISTICAL ANALYSIS

SUPPLEMENTAL INFORMATION

Supplemental Information can be found online at https://doi.org/10.1016/j.celrep.2020.107533.

ACKNOWLEDGMENTS

We thank members of the Hickson laboratory for helpful discussions and Andrés López-Contreras for the plasmid to knock out *TP53*. Work in the Hickson

laboratory is supported by the Danish National Research Foundation (DNRF115) and the Nordea Foundation. A.B.V. was supported by a PhD fellowship from the Lundbeck Foundation (R208-2015-3785). Work in the Kanemaki laboratory is supported by KAKENHI grants from the Japan Society for the Promotion of Science (JSPS) (17K15068, 18H02170, 18H04719, and 19K06495), the Mochida Memorial Foundation for Medical and Pharmaceutical Research, the Daiichi Sankyo Foundation of Life Science, the Sumitomo Foundation, the Inamori Foundation, the Asahi Glass Foundation, and the Takeda Science Foundation.

AUTHOR CONTRIBUTIONS

A.B.V. designed and conducted experiments with input from I.D.H. Degron cell lines were generated by T.N. and M.K. A.B.V. and I.D.H wrote the manuscript, and all authors reviewed and edited it.

DECLARATION OF INTERESTS

The authors declare no competing interests.

Received: October 28, 2019
Revised: February 11, 2020
Accepted: March 27, 2020
Published: April 21, 2020

REFERENCES

Aragón, L. (2018). The Smc5/6 complex: new and old functions of the enigmatic long-distance relative. Annu. Rev. Genet. *52*, 89–107.

Behlke-Steinert, S., Touat-Todeschini, L., Skoufias, D.A., and Margolis, R.L. (2009). SMC5 and MMS21 are required for chromosome cohesion and mitotic progression. Cell Cycle *8*, 2211–2218.

Bermúdez-López, M., Ceschia, A., de Piccoli, G., Colomina, N., Pasero, P., Aragón, L., and Torres-Rosell, J. (2010). The Smc5/6 complex is required for dissolution of DNA-mediated sister chromatid linkages. Nucleic Acids Res. *38*, 6502–6512.

Bermúdez-López, M., Pociño-Merino, I., Sánchez, H., Bueno, A., Guasch, C., Almedawar, S., Bru-Virgili, S., Garí, E., Wyman, C., Reverter, D., et al. (2015). ATPase-dependent control of the Mms21 SUMO ligase during DNA repair. PLoS Biol. *13*, e1002089.

Bermúdez-López, M., Villoria, M.T., Esteras, M., Jarmuz, A., Torres-Rosell, J., Clemente-Blanco, A., and Aragon, L. (2016). Sgs1's roles in DNA end resection, HJ dissolution, and crossover suppression require a two-step SUMO regulation dependent on Smc5/6. Genes Dev. *30*, 1339–1356.

Bhowmick, R., Minocherhomji, S., and Hickson, I.D. (2016). RAD52 facilitates mitotic DNA synthesis following replication stress. Mol. Cell *64*, 1117–1126.

Bonner, J.N., Choi, K., Xue, X., Torres, N.P., Szakal, B., Wei, L., Wan, B., Arter, M., Matos, J., Sung, P., et al. (2016). Smc5/6 mediated sumoylation of the Sgs1-Top3-Rmi1 complex promotes removal of recombination intermediates. Cell Rep. *16*, 368–378.

Chang, E.Y.-C., Tsai, S., Aristizabal, M.J., Wells, J.P., Coulombe, Y., Busatto, F.F., Chan, Y.A., Kumar, A., Dan Zhu, Y., Wang, A.Y.-H., et al. (2019). MRE11-RAD50-NBS1 promotes Fanconi anemia R-loop suppression at transcription-replication conflicts. Nat. Commun. *10*, 4265.

Chen, Y.-H., Choi, K., Szakal, B., Arenz, J., Duan, X., Ye, H., Branzei, D., and Zhao, X. (2009). Interplay between the Smc5/6 complex and the Mph1 helicase in recombinational repair. Proc. Natl. Acad. Sci. U S A *106*, 21252–21257.

Chu, W.K., and Hickson, I.D. (2009). RecQ helicases: multifunctional genome caretakers. Nat. Rev. Cancer *9*, 644–654.

De Piccoli, G., Cortes-Ledesma, F., Ira, G., Torres-Rosell, J., Uhle, S., Farmer, S., Hwang, J.Y., Machin, F., Ceschia, A., McAleenan, A., et al. (2006). Smc5-Smc6 mediate DNA double-strand-break repair by promoting sister-chromatid recombination. Nat. Cell Biol. *8*, 1032–1034.

Deiss, K., Lockwood, N., Howell, M., Segeren, H.A., Saunders, R.E., Chakravarty, P., Soliman, T.N., Martini, S., Rocha, N., Semple, R., et al. (2019). A genome-wide RNAi screen identifies the SMC5/6 complex as a non-redundant regulator of a Topo2a-dependent G2 arrest. Nucleic Acids Res. *47*, 2906–2921.

Doyle, J.M., Gao, J., Wang, J., Yang, M., and Potts, P.R. (2010). MAGE-RING protein complexes comprise a family of E3 ubiquitin ligases. Mol. Cell *39*, 963–974.

Duan, X., Sarangi, P., Liu, X., Rangi, G.K., Zhao, X., and Ye, H. (2009). Structural and functional insights into the roles of the Mms21 subunit of the Smc5/6 complex. Mol. Cell *35*, 657–668.

Fernandez-Capetillo, O. (2016). The (elusive) role of the SMC5/6 complex. Cell Cycle *15*, 775–776.

Gallego-Paez, L.M., Tanaka, H., Bando, M., Takahashi, M., Nozaki, N., Nakato, R., Shirahige, K., and Hirota, T. (2014). Smc5/6-mediated regulation of replication progression contributes to chromosome assembly during mitosis in human cells. Mol. Biol. Cell *25*, 302–317.

Glück, S., Guey, B., Gulen, M.F., Wolter, K., Kang, T.W., Schmacke, N.A., Bridgeman, A., Rehwinkel, J., Zender, L., and Ablasser, A. (2017). Innate immune sensing of cytosolic chromatin fragments through cGAS promotes senescence. Nat. Cell Biol. *19*, 1061–1070.

Harvey, S.H., Sheedy, D.M., Cuddihy, A.R., and O'Connell, M.J. (2004). Coordination of DNA damage responses via the Smc5/Smc6 complex. Mol. Cell. Biol. *24*, 662–674.

Jacome, A., Gutierrez-Martinez, P., Schiavoni, F., Tenaglia, E., Martinez, P., Rodríguez-Acebes, S., Lecona, E., Murga, M., Méndez, J., Blasco, M.A., and Fernandez-Capetillo, O. (2015). NSMCE2 suppresses cancer and aging in mice independently of its SUMO ligase activity. EMBO J. *34*, 2604–2619.

Ju, L., Wing, J., Taylor, E., Brandt, R., Slijepcevic, P., Horsch, M., Rathkolb, B., Rácz, I., Becker, L., Hans, W., et al. (2013). SMC6 is an essential gene in mice, but a hypomorphic mutant in the ATPase domain has a mild phenotype with a range of subtle abnormalities. DNA Repair (Amst.) *12*, 356–366.

Kegel, A., Betts-Lindroos, H., Kanno, T., Jeppsson, K., Ström, L., Katou, Y., Itoh, T., Shirahige, K., and Sjögren, C. (2011). Chromosome length influences replication-induced topological stress. Nature *471*, 392–396.

Kliszczak, M., Stephan, A.K., Flanagan, A.M., and Morrison, C.G. (2012). SUMO ligase activity of vertebrate Mms21/Nse2 is required for efficient DNA repair but not for Smc5/6 complex stability. DNA Repair (Amst.) *11*, 799–810.

Lehmann, A.R., Walicka, M., Griffiths, D.J., Murray, J.M., Watts, F.Z., McCready, S., and Carr, A.M. (1995). The rad18 gene of Schizosaccharomyces pombe defines a new subgroup of the SMC superfamily involved in DNA repair. Mol. Cell. Biol. *15*, 7067–7080.

Lindroos, H.B., Ström, L., Itoh, T., Katou, Y., Shirahige, K., and Sjögren, C. (2006). Chromosomal association of the Smc5/6 complex reveals that it functions in differently regulated pathways. Mol. Cell *22*, 755–767.

Menolfi, D., Delamarre, A., Lengronne, A., Pasero, P., and Branzei, D. (2015). Essential roles of the Smc5/6 complex in replication through natural pausing sites and endogenous DNA damage tolerance. Mol. Cell *60*, 835–846.

Minocherhomji, S., Ying, S., Bjerregaard, V.A., Bursomanno, S., Aleliunaite, A., Wu, W., Mankouri, H.W., Shen, H., Liu, Y., and Hickson, I.D. (2015). Replication stress activates DNA repair synthesis in mitosis. Nature *528*, 286–290.

Natsume, T., Kiyomitsu, T., Saga, Y., and Kanemaki, M.T. (2016). Rapid protein depletion in human cells by auxin-inducible degron tagging with short homology donors. Cell Rep. *15*, 210–218.

Payne, F., Colnaghi, R., Rocha, N., Seth, A., Harris, J., Carpenter, G., Bottomley, W.E., Wheeler, E., Wong, S., Saudek, V., et al. (2014). Hypomorphism in human NSMCE2 linked to primordial dwarfism and insulin resistance. J. Clin. Invest. *124*, 4028–4038.

Peng, X.P., Lim, S., Li, S., Marjavaara, L., Chabes, A., and Zhao, X. (2018). Acute Smc5/6 depletion reveals its primary role in rDNA replication by restraining recombination at fork pausing sites. PLoS Genet. *14*, e1007129.

Pond, K.W., de Renty, C., Yagle, M.K., and Ellis, N.A. (2019). Rescue of collapsed replication forks is dependent on NSMCE2 to prevent mitotic DNA damage. PLoS Genet. *15*, e1007942.

Potts, P.R., and Yu, H. (2005). Human MMS21/NSE2 is a SUMO ligase required for DNA repair. Mol. Cell. Biol. *25*, 7021–7032.

Potts, P.R., and Yu, H. (2007). The SMC5/6 complex maintains telomere length in ALT cancer cells through SUMOylation of telomere-binding proteins. Nat. Struct. Mol. Biol. *14*, 581–590.

Ran, F.A., Hsu, P.D., Wright, J., Agarwala, V., Scott, D.A., and Zhang, F. (2013). Genome engineering using the CRISPR-Cas9 system. Nat. Protoc. *8*, 2281–2308.

Räschle, M., Smeenk, G., Hansen, R.K., Temu, T., Oka, Y., Hein, M.Y., Nagaraj, N., Long, D.T., Walter, J.C., Hofmann, K., et al. (2015). Proteomics reveals dynamic assembly of repair complexes during bypass of DNA cross-links. Science *348*, 1253671.

Saldivar, J.C., Hamperl, S., Bocek, M.J., Chung, M., Bass, T.E., Cisneros-Soberanis, F., Samejima, K., Xie, L., Paulson, J.R., Earnshaw, W.C., et al. (2018). An intrinsic S/G 2 checkpoint enforced by ATR. Science *361*, 806–810.

Stephan, A.K., Kliszczak, M., Dodson, H., Cooley, C., and Morrison, C.G. (2011). Roles of vertebrate Smc5 in sister chromatid cohesion and homologous recombinational repair. Mol. Cell. Biol. *31*, 1369–1381.

Torres-Rosell, J., Machín, F., Farmer, S., Jarmuz, A., Eydmann, T., Dalgaard, J.Z., and Aragón, L. (2005). SMC5 and SMC6 genes are required for the segregation of repetitive chromosome regions. Nat. Cell Biol. *7*, 412–419.

Torres-Rosell, J., De Piccoli, G., Cordon-Preciado, V., Farmer, S., Jarmuz, A., Machin, F., Pasero, P., Lisby, M., Haber, J.E., and Aragón, L. (2007). Anaphase onset before complete DNA replication with intact checkpoint responses. Science *315*, 1411–1415.

van der Crabben, S.N., Hennus, M.P., McGregor, G.A., Ritter, D.I., Nagamani, S.C.S., Wells, O.S., Harakalova, M., Chinn, I.K., Alt, A., Vondrova, L., et al. (2016). Destabilized SMC5/6 complex leads to chromosome breakage syndrome with severe lung disease. J. Clin. Invest. *126*, 2881–2892.

Wu, N., and Yu, H. (2012). The Smc complexes in DNA damage response. Cell Biosci. *2*, 5.

Zhang, B.N., Bueno Venegas, A., Hickson, I.D., and Chu, W.K. (2019). DNA replication stress and its impact on chromosome segregation and tumorigenesis. Semin. Cancer Biol. *55*, 61–69.

STAR★METHODS

KEY RESOURCES TABLE

REAGENT or RESOURCE	SOURCE	IDENTIFIER
Antibodies		
Rabbit anti-GFP (1:500, IF)	Abcam	Cat# ab13970, RRID:AB_300798
Mouse anti-UBF (1:200, IF)	Santa Cruz Biotechnology	Cat# sc-13125, RRID:AB_671403
Rabbit anti-UBTF (1:400, IF)	Novus Biologicals	Cat# NBP1-82545, RRID:AB_11032609
Human autoantibody against centromere (CREST) (1:1000, IF)	Erba Diagnostics	Cat# HCT-0100, RRID:AB_2744669
Guinea pig anti-PICH (1:200, IF)	Purified in House	Not available
Rabbit anti-Histone H3, phospho (S10) (1:5000, WB and 1:1000, IF)	Merck Millipore	Cat# 06-570, RRID:AB_310177
Mouse anti-α-tubulin (1:5000, WB and 1:1000, IF)	Sigma-Aldrich	Cat# T5168, RRID:AB_477579
Rabbit anti-lamin A (1:500, IF)	Abcam	Cat# ab26300, RRID:AB_775965
Mouse anti-SMC6 (1:1000, WB)	Santa Cruz Biotechnology	Cat# sc-365742, RRID:AB_10846328
Rabbit anti-SMC5 (1:1000, WB)	Novus Biologicals	Cat# NB100-469, RRID:AB 2192776
Rabbit anti-NSMCE4A (1:1000, WB)	Sigma-Aldrich	Cat# HPA037459, RRID:AB_10696932
Rabbit anti-GAPDH (1:2000, WB)	Bethyl Laboratories	Cat# A300-639A, RRID:AB_513616
Mouse anti-p53 (1:1000, WB)	Santa Cruz Biotechnology	Cat# sc-126, RRID:AB_628082
Rabbit anti-p21 (1:1000, WB)	Cell Signaling	Cat# 2947, RRID:AB_823586
Mouse anti-CHK2 (1:500, WB)	Santa Cruz Biotechnology	Cat# sc-17747, RRID:AB_627258
Rabbit anti-CHK2, phospho (T68) (1:1000, WB)	Cell Signaling	Cat# 2661, RRID:AB_331479
Mouse anti-CHK1 (1:500, WB)	Santa Cruz Biotechnology	Cat# sc-8408, RRID:AB_627257
Rabbit anti-CHK1, phospho (S345) (1:1000, WB)	Cell Signaling	Cat# 2341, RRID:AB_330023
Rabbit anti-H2B (1:5000, WB and 1:1000 IF)	Abcam	Cat# ab1790, RRID:AB_302612
Rabbit anti-FOXM1, phospho (T600) (1:1000, WB)	Cell Signaling	Cat# 14655, RRID:AB_2798557
Rabbit anti-SMC3 (1:1000, WB)	Abcam	Cat# ab128919, RRID:AB_11150430
Goat anti-TOP2α (1:500, WB)	Santa Cruz Biotechnology	Not available
Mouse anti-TOP2α (1:100, IF)	MBL International	Cat# M042-3, RRID:AB_592889
Rabbit anti-SMC2 (1:1000, WB)	Abcam	Cat# ab10412, RRID:AB_2192486
Guinea pig anti-CENPC (1:1000, IF)	MBL International	Cat# PD030, RRID:AB_10693556
Mouse anti-Cyclin A (1:500, IF)	Santa Cruz Biotechnology	Cat# sc-271682, RRID:AB_10709300
Rat anti-BrdU (1:200, IF)	Abcam	Cat# ab6326, RRID:AB_305426
Mouse anti-BrdU (1:200, IF)	BD Biosciences	Cat# 347580, RRID:AB_400326
Mouse anti-γH2A.X (1:200, IF)	Millipore	Cat# 05-636, RRID:AB_309864
Goat anti-mouse (H+L)-Peroxidase (1:500, WB)	Sigma-Aldrich	Cat# A-4416, RRID: AB_258167
Goat anti-rabbit (H+L)-Peroxidase (1:5000, WB)	Sigma-Aldrich	Cat# A-6667, RRID:AB_258307
Alexa Fluor 488 goat anti-mouse IgG (1:500, IF)	Thermo Fisher	Cat# A-11008, RRID:AB_143165
Alexa Fluor 488 goat anti-rabbit IgG (1:500, IF)	Thermo Fisher	Cat# A-11001, RRID:AB_2534069
Alexa Fluor 568 goat anti-mouse IgG (1:500, IF)	Thermo Fisher	Cat# A-11004, RRID:AB_2534072

(*Continued on next page*)

Continued

REAGENT or RESOURCE	SOURCE	IDENTIFIER
Alexa Fluor 568 goat anti-guinea pig IgG (1:500, IF)	Thermo Fisher	Cat# A-11075, RRID:AB 2534119
Alexa Fluor 568 goat anti-rabbit IgG (1:500, IF)	Thermo Fisher	Cat# A-11011, RRID:AB_143157
Alexa Fluor 647 goat anti-human IgG (1:500, IF)	Thermo Fisher	Cat# A-21445, RRID:AB_2535862
Alexa Fluor 647 goat anti-guinea pig IgG (1:500, IF)	Thermo Fisher	Cat# A-21450, RRID:AB_2735091
Chemicals, Peptides, and Recombinant Proteins		
RO-33O6 (7 μM)	APExBIO	Cat# 8885
Nocodazole (3.3 μM)	Sigma-Aldrich	Cat# M1404
Doxycycline (100 ng/mL)	Thermo Fisher	Cat# 10687010
3-Indole-acetic acid (IAA) (500 μM)	Abcam	Cat# ab146402
Lovastatin (20 mM)	SelleckChem	Cat# S2061
(±)-Mevalonolactone (2 mM)	Sigma-Aldrich	Cat# M4667
Experimental Models: Cell Lines		
HCT116	ATCC	ATCC Cat# CCL-247, RRID:CVCL 0291
HCT116 CMV-OsTIR1	Natsume et al., 2016	Not available
HCT116 NSE4A-mAID	This Study	Not available
HCT116 NSE4A-/SMC6-mAID	This Study	Not available
HCT116 Tet-OsTIR1	Natsume et al., 2016	Not available
HCT116 Tet-OsTIR1 SMC6-mAID-Clover	This Study	Not available
hTERT-RPE1 Tet-OsTIR1 SMC6-mAID	This Study	Not available
Oligonucleotides		
sgRNA targeting last exon of *NSE4A*: TTCAGCTAGCATCAAGCACT	Not available	Not available
sgRNA targeting last exon of *SMC6*: GTTAAGTTACAAATCACCTT	Not available	Not available
Software and Algorithms		
GraphPad Prism 7	Graphpad	Not available
FIJI	ImageJ	Not available

RESOURCE AVAILABILITY

Lead Contact

Further information and requests for resources and reagents should be directed to and will be fulfilled by the Lead Contact, Ian D. Hickson (iandh@sund.ku.dk).

Materials Availability

All plasmids and cell lines generated in this study are available from the Lead Contact without restriction.

Data and Code Availability

Original/source data for each figure in the paper has been deposited in Mendeley (https://doi.org/10.17632/khmcnx9f22.2). This study did not generate any unique code.

EXPERIMENTAL MODEL AND SUBJECT DETAILS

HCT116 cells expressing either CMV-OsTIR1 or Tet-OsTIR1 from the AAVS1 locus were generated as described previously (Natsume et al., 2016). Clones with homozygous insertions at the AAVS1 locus were used to make the different degron cell lines used in the study. HCT116 CMV-OsTIR1 NSE4A-mAID were generated by co-transfecting HCT116 CMV-OsTIR1 with pX330-NSE4A-C and NSE4A-mAID-Hygro donor. After selection with 100 μg/mL HygroGold, single colonies were isolated and homologous recombination mediated *knock-in* of mAID at both NSE4A alleles was confirmed by genomic PCR and western blotting. To generate

HCT116 CMV-OsTIR1 NSE4A-mAID SMC6-mAID cells, HCT116 CMV-OsTIR1 NSE4-mAID cells were co-transfected with pX330-SMC6-C and SMC6-mAID-Neo donor. After selection with 700 μg/mL G418, single colonies were isolated and homologous recombination *knock-in* of mAID at both SMC6 alleles was confirmed by genomic PCR and western blot. HCT116 Tet-OsTIR1 SMC6-mAID-mClover (-mAC) was generated by co-transfecting HCT116 Tet-OsTIR1 cells with pX330-SMC6-C and SMC6-mAID-mClover-Hygro donor. After selection with 100 μg/mL HygroGold, colonies were isolated and homozygous insertions of the -mAC epitope at the C terminus of both SMC6 alleles were confirmed by genomic PCR and western blot. To generate HCT116 CMV-OsTIR1 NSE4A-mAID SMC6-mAID *TP53*$^{-/-}$ the following sgRNA sequence: 5′-GTCAGTCTAGGA TCGCAGCT-3′ targeting the exon 2 of *TP53* gene was cloned into the pSpCas9(BB)-2A-GFP plasmid (PX458, Addgene plasmid #48138) (Ran et al., 2013). The resulting plasmid was transfected into CMV-OsTIR1 NSE4A-mAID SMC6-mAID and, 48h later, GFP positive cells were single sorted into 96-well plates. Different clones were expanded and expression of p53 was assessed by western blot after treatment with 2 μM doxorubicin for 5h. Negative clones for p53 were selected for further analysis.

hTERT-RPE1 cells expressing Tet-OsTIR1 from the ROSA26 locus were generated by co-electroporating hTERT-RPE1 (puromycin-sensitive, a gift from Helfrid Hochegger) with pX330-ROSA26 and ROSA26-Tet-OsTIR1-Puro. After selection with 2 μg/mL puromycin, single colonies were isolated and homologous recombination mediated *knock-in* of the Tet-OsTIR1-Puro expression construct at one ROSA26 allele was confirmed by genomic PCR and western blotting. To generate RPE-1 Tet-OsTIR1 SMC6-mAID cells, RPE-1 Tet-OsTIR1 cells were co-electroporated with pX330-SMC6-C and SMC6-mAID-Neo donor. After selection with 1000 μg/mL G418, single colonies were isolated and homologous recombination *knock-in* of mAID at both SMC6 alleles was confirmed by genomic PCR and western blot.

All cell lines were cultured in Dulbecco's Modified Eagle Medium (DMEM, Thermo Fisher Scientific) supplemented with 10% fetal bovine serum (FBS, Invitrogen, Cat# 10500), 100 U/mL penicillin and 100 mg/mL streptomycin. Cells were grown at 37°C in a humidified atmosphere containing 5% CO_2 and were screened regularly for being mycoplasma-free.

METHOD DETAILS

Colony formation assays

250 or 2500 cells were seeded into 6-well plates, and 24h later the medium was replaced with fresh medium containing either $_{dd}H_2O$ or 500 μM 3-indole-acetic acid (IAA). The medium was replaced every 24h. After 10 days, colonies were washed with pre-warmed PBS 1X and were fixed in 20% methanol/0.5% w/v crystal violet for 20 min at room temperature. Fixed colonies were washed with PBS 1X and $_{dd}H_2O$, and then allowed to dry. The colonies were counted automatically using FIJI.

Cell synchronization

For cell cycle arrest in G1, cells growing either on coverslips or in flasks were incubated with lovastatin at a final concentration of 20 μM for 24h. To induce degradation of the different subunits of the SMC5/6 complex in G1, IAA was added to a final concentration of 500 μM 4h prior releasing the cells from the lovastatin blockade. Cells were released from G1 by washing three times with pre-warmed DMEM. Cells were allowed to enter into the cell cycle either in the absence or presence of IAA and 2 mM mevalonate (Sigma-Aldrich). For cell cycle arrest in G2, cells released from lovastatin for 18h were treated with the CDK1 inhibitor RO-3306 (7 μM) for 3h. To induce degradation of both NSE4A-mAID and SMC6-mAID at this stage, IAA was added at the same time as RO-3306. To assess segregation problems during anaphase, G2-arrested cells were released for 42 min and fixed. For mitotic spreads, cells were instead released into 3.33 μM nocodazole for 1h.

Chromosome spreads and centromeric FISH

After the stated treatments, cells were collected by trypsinization, washed once with ice-cold DPBS 1X, homogenized in 5 mL ice-cold 75 mM KCl, and were incubated on ice for 10 min. Cells were then centrifuged at 300 *rcfs* for 5 min at 4°C, washed with 75 mM KCl and incubated on ice for an additional 10 min. After centrifugation, swollen cells were homogenized in a small volume of 75 mM KCl (typically 0.2-0.5 mL) and were fixed by the addition of ice-cold methanol/acetic acid (3/1) dropwise while vortexing at slow speed. Fixed cells were kept at −20°C overnight. The day after, cells were washed 4-5 times with ice-cold methanol/acetic acid, homogenized in a small volume and spread on tilted glass slides. Slides were then dipped in methanol/acetic acid for 2h at room temperature, air-dried, hydrated in PBS 1X for 5 min and were then fixed with 3.7% formaldehyde/PBS 1X for 10 min at room temperature. After washing three times with PBS 1X for a total of 15 min, slides were dehydrated in series of cold ethanol and air-dried. Slides were then incubated with a PNA probe specific for CENP-B box DNA (1:50, PNA Bio, Cat# F3001) in 70% formamide, 25 mM $MgCl_2$, 10 mM tris-HCl pH 7.4 for 3 min at 80°C (protected from the light), followed by an incubation of 2h at 37°C in a humidified chamber. After hybridization, slides were washed three times in 2X SSC/0.1% tween-20 for a total of 15 min, three times in 1X SSC, rinsed with DNase/RNase-free H_2O, dehydrated in series of cold ethanol, allowed to air dry and mounted with Vecta Shield anti-fade mounting medium containing DAPI.

Cell cycle analysis

After indicated treatments, cells were collected by trypsinization, washed once with DPBS 1X and homogenized in a small volume of DPBS 1X, typically 0.25-0.5 mL, before being fixed with −20°C 70% ethanol, which was added dropwise while vortexing at low

speed. Fixed cells were kept for at least 2h at −20°C before being processed. After fixation, ethanol was removed by centrifugation at 500 *rcfs* for 5 min at 4°C and cells were washed two to three times with DPBS 1X supplemented with 1% BSA. Finally, cells were resuspended in 1 mL DPBS 1X-containing 0.04 mg/mL Propidium Iodide and 0.1 mg/mL RNase A and then incubated at 37°C for 45-60 min. Cell cycle distribution analysis was performed on a FACS Calibur flow cytometer (BD Biosciences). 25000 cells were counted per condition and data analysis was carried out by using the Cell Quest Pro software.

Preparation of protein extracts and western blotting

Cells growing in T25 flasks or 6-well plates were either collected by trypsinization or washed once with ice-cold DPBS 1X and scraped with a cell strainer in the presence of 1-3 mL ice-cold DPBS 1X. After 5 min of centrifugation at 500 *rcfs* at 4°C, cell pellets were either snap frozen on dry ice or lysed by the addition of 150-200 μL of Nuclear Extraction Buffer (50 mM tris-HCl pH 8, 500 mM NaCl, 10% glycerol, 1% NP-40, 0.1% SDS, 1 mM DTT, 0.5% sodium deoxycholate) complemented with Protease Inhibitor Cocktail (Roche, Cat# 11836153001) and phosphatase inhibitors, PhoSTOP (Roche, Cat# 04906837001). Cell extracts were incubated on ice for 30 min with regular vortexing and sonicated five times using a 30 s ON, 30 s OFF pulse in a Bioruptor Pico sonicator. The soluble fraction was collected after centrifugation at > 20,000 *rcfs* for 20 min at 4°C, and the protein concentration measured using the Pierce™ BCA protein assay kit (Thermo Fisher Scientific, Cat# 23227). Samples were boiled for 5 min at 95°C in NuPAGE® LDS Sample Buffer containing 100 mM DTT. Unless otherwise stated, 30 μg of protein was loaded per sample. Proteins resolved on 4%–12% Bis-Tris gel were transferred to a high-bond PVDF membrane. The membrane was blocked in 0.1% tween 20/PBS supplemented with 5% milk or 5% BSA (for detection of some phosphorylated proteins such as CHK2-T68p or CHK1-S345p) for 1h at room temperature and incubated with the appropriate antibodies for at least 2h at room temperature or overnight at 4°C. The membrane was washed three times in 0.1% tween 20/PBS for 30 min. The membrane was incubated with appropriate secondary antibodies in the presence of 0.1% tween 20/PBS containing 0.25%–5% milk for 1-2h at room temperature. After three washes in 0.1% tween 20/PBS, the membrane was developed using ECL.

Chromatin fractionation

Cells growing on 10 cm dishes were washed once with DPBS 1X and trypsinized. Cells were spun at 300 *rcfs* for 5 min at 4°C and homogenized in buffer A (300 mM sucrose, 100 mM NaCl, 10 mM PIPES-NaOH pH 6.8, 3 mM $MgCl_2$, 1 mM EGTA, 0.2% Triton X-100 mM) complemented with Protease Inhibitor Cocktail (Roche, Cat# 11836153001) and phosphatase inhibitors, PhoSTOP (Roche, Cat# 04906837001). Cells were incubated on ice for 5 min and centrifuged at 1000 *rcfs* for 5 min at 4°C. The supernatant was kept (soluble fraction) and the resulting pellet was washed once more with buffer A and homogenized in buffer B (50 mM tris-HCl pH 7.5, 500 mM NaCl, 10% glycerol, 1% Triton X-100, 0.5% sodium deoxycholate, 0.1% SDS, 1 mM DTT, 5 mM EDTA) complemented with PIC and PhoSTOP, incubated on ice for 30 min with regular vortexing, and sonicated five times using a 30 s ON, 30 s OFF pulse in a Bioruptor Pico sonicator. Chromatin extracts were centrifuged at > 20.000 *rcfs* for 20 min at 4°C and the resulting fraction containing the chromatin bound proteins was kept. Samples were boiled for 5 min at 95°C in NuPAGE® LDS Sample Buffer containing 100 mM DTT and 20-30 μg of protein was loaded per sample.

DNA fibers

After specified treatments, cells were pulsed labeled with 25 μM CldU for 20 min, washed twice with pre-warmed medium, and then pulsed labeled with 250 μM IdU for an additional 20 min. Cells were washed three times with ice-cold DPBS 1X and collected by trypsinization. Cell pellets were homogenized in DPBS 1X to a final concentration of 2500 cells/μL. Four μL of cells were directly lysed on microscope slides by adding 8 μL of spreading buffer (0.5% sodium dodecyl sulfate, 200 mM tris-HCl pH 7.5, 50 mM EDTA). After 2 min incubation at room temperature, the slides were tilted by 15°, and the drop was allowed to slide down slowly for 2 to 5 min. The slides were briefly air-dried for 10 min and then fixed in methanol/acetic acid (3/1) for 10 min. After fixation, the slides were washed three times in PBS 1X, washed once with 2.5 M HCl and denatured for 80 min at room temperature with 2.5 M HCl. After denaturation, the slides were washed four times in PBS 1X, once with 0.1% Triton X-100/1%BSA/PBS 1X and were then blocked in the same buffer for 30 min at room temperature. Slides were subsequently incubated with rat anti-BrdU (1:200 in blocking buffer) for 75 min at room temperature, washed once with 0.1% tween/PBS 1X, twice with PBS 1X and were then crosslinked in 4% formaldehyde/PBS 1X for 10 min. The slides were washed three times in PBS 1X and incubated for 60 min at room temperature with anti-rat Alexa Fluor 568 (1:100 in blocking buffer), washed again three times with PBS 1X and incubated overnight at 4°C with mouse anti-BrdU (1:200). The day after the slides were washed once with 0.1% tween/PBS 1X, twice with PBS 1X and incubated with anti-mouse Alexa Fluor 488 (1:100) for 60 min at room temperature. Finally, slides were washed five times with PBS 1X and mounted using Vecta Shield anti-fade mounting medium.

Immunofluorescence

Following various treatments, cells grown on coverslips were washed once with pre-warmed PBS 1X and fixed with PMEF (20 mM PIPES-NaOH pH 6.8, 10 mM EGTA, 1 mM $MgCl_2$, 3.7% formaldehyde) for 10 min at room temperature. For staining of proteins bound to chromatin, cells were instead, pre-extracted with PME containing 0.2% Triton X-100 for 1 min at room temperature, followed by fixation with formaldehyde 3.7% for 10 min at room temperature. After fixation, cells were washed three times with PBS 1X at room temperature and permeabilized (only when Triton X-100 was absent in the fixation buffer) with 0.15% Triton X-100/PBS 1X for 10 min

at room temperature. Cells were blocked in DMEM containing 10% FBS and 5% BSA for at least 1h at room temperature or overnight at 4°C. After blocking, cells were incubated with indicated primary antibodies overnight at 4°C in a humidified chamber. The day after, cells were washed three times with 0.1% tween-20/PBS 1X at room temperature and incubated with indicated Alexa Fluor coupled secondary antibodies for 1-2h at room temperature and protected from light. Cells were washed three times with 0.1% tween-20/PBS 1X, counterstained with DAPI (0.2 μg/mL) and then mounted on glass slides using Vecta Shield anti-fade mounting medium.

QUANTIFICATION AND STATISTICAL ANALYSIS

No statistical methods were used to pre-determine sample size. The experiments were not randomized, and the investigators were not blinded to allocation during experiments and outcome assessment. Unless stated, at least three independent experiments were carried out to generate each dataset. All graphical representations of data and statistical analyses were performed using GraphPad Prism. Error bars represent standard deviation (SD). The number of cells quantified for each experiment as well as the number of biological replicates and *p* values are indicated in figures or figure legends.